NRC Publications Archive
Archives des publications du CNRC

Copper immersion deposition on magnesium alloy: the effect of fluoride and temperature
Yang, Lianxi; Luan, Ben

NRC Publications Record / Notice d'Archives des publications de CNRC:
https://nrc-publications.canada.ca/eng/view/object/?id=7997ba7b-b33c-40c6-81be-87b2bdbe037(
https://publications-cnrc.canada.ca/fra/voir/objet/?id=7997ba7b-b33c-40c6-81be-87b2bdbe0370

National Research Council Canada   Conseil national de recherches Canada

Canada

Copper immersion deposition on magnesium alloy – the effect of fluoride and temperature

Lianxi Yang and Ben Luan*

Integrated Manufacturing Technologies Institute, National

Research Council Canada, 800 Collip Circle, London, Ontario,

Canada N5G 4X8

Abstract - A study was carried out to examine copper immersion deposition on AZ91 magnesium alloy in a hydrofluoric acid containing bath. The role of fluoride and the effect of bath temperature were investigated. The study was performed by measuring the AC impedance and open circuit potentials in combination with surface analysis of XPS, SEM and EDS. Results showed that the effect of both HF concentration and temperature on surface coverage is significant, via affecting the surface film formation on the uncoated areas of magnesium surface. The surface film composed of an outer layer rich in fluorine (MgF_2-

$Mg(OH)_{2-x}F_x$), an intermediate layer of $Mg-Al(OH)_{2-x}F_x$, and an inner layer of Mg-Al oxide rich in aluminum. A model for understanding the copper immersion coating process is also depicted, based on the surface characterization of this film and the electrochemical measurements.

* Corresponding author. Tel.: 1-519-430-7043, fax: 1-519-430-7064, Email: Ben.luan@nrc.gc.ca

1. Introduction

Magnesium alloys fulfills many technical requirements for engineering applications with a combination of high specific strength, good machinability and excellent castability, and high recycling potential. The automotive industry leads the way in the growing interest in magnesium alloys for further reduction of emissions to lower the growing environmental impact [1].

However, the poor wear and corrosion properties of magnesium alloys are the major hindering in their wide use. In fact, magnesium is intrinsically highly reactive and its alloys usually have poor corrosion resistance [2-4], particularly with the internal galvanic corrosion caused by second phases [5], the poor stability of the quasi-passive hydroxide surface film [4] and the film imperfections [6]. Surface coatings are therefore needed for the effective application of magnesium alloys in industry [7].

It general, electroless deposition on magnesium alloy is a good candidate with combined advantages such as excellent uniformity,

high corrosion and wear resistances and excellent scalability [7]. A number of studies have reported on the plating techniques, including indirect and direct electroless deposition [8-12]. For the indirect electroless coating, a zinc immersion pretreatment process is used, followed by cyanide strike, prior to electorless plating. The process has been criticized for the requirement of precise control to ensure adequate adhesion. In many cases non-uniform coverage on the surface is seen with spongy non-adherent zinc deposits on the intermetallic phase of the base alloys. A copper cyanide strike that must follow has also been of concern [13]. For direct electroless deposition on magnesium alloy, dissolution of magnesium causes contamination, which leads to the decomposition of electroless plating solution, a major challenge for its industrial application.

Our recent research has focused on a simple copper immersion coating on AZ91 magnesium alloy in a hydrofluoric acid bath [14]. This process has an advantage with respect to the reduced cost, increased coating uniformity, simple operation, and excellent scalability. Furthermore, the copper immersion coated magnesium

surface is feasible for subsequent engineering coatings such as electrodeposition of copper.

The copper immersion coating on magnesium involves charge transfer between reacting chemical species of Mg/Mg^{++}, Cu/Cu^{++}. More specifically [15],

$$\text{Anodic:} \quad Mg = Mg^{2+} + 2e \qquad E^o = -2.375 \qquad (1)$$

$$\text{Cathodic} \quad Cu^{2+} + 2e = Cu \qquad E^o = +0.340 \qquad (2)$$

In addition, hydrogen evolution occurs as a by-reaction of cathodic reductions. During the immersion coating, the surface of magnesium substrate consists of a mosaic of anodic and cathodic sites. The copper deposition simultaneously results as the magnesium dissolution occurs. Theoretically, the process will continue until the entire substrate is covered with copper. However, in the aqueous bath containing copper ions, the copper coating process was accompanied by violent gas evolution and

magnesium dissolution, impeding the development of good quality coating. The production of a continuous deposit of copper on aluminum alloys has already been produced by using a slightly acidic bath containing the copper partly or completely in complexion bounding to oxalic group [16,17] and to tartrate [18,19]. However, this approach has not been applied on magnesium alloy, to the best of our knowledge. Our previous paper [14] shows that for applying copper deposition to magnesium alloy, the presence of fluoride in the bath is essential as it plays a dominating role in increasing the copper surface coverage.

This paper explores the mechanism of copper immersion coating processes with regard to the role of fluoride and the effect of bath temperature. The study is performed by measuring the AC impedance and open circuit potential in combination with surface analysis of XPS, SEM and EDS.

2. Experimental

2.1. Materials and chemicals

The magnesium alloy substrate used throughout the experiments in this study was the AZ91 magnesium alloy (including AZ91D and AZ91E). Its nominal composition is shown in Table 1. All the chemicals (AR grade), including NaOH, Na_2CO_3, Na_3PO_4, HF, $CuSO_4$ and $(CH_3)_2CHOH$ were supplied by Sigma. In this study, De-ionized water (> 15 $M\Omega$ cm^{-1}) prepared with Millipore Elix 10 Water Deionization system was used for solution preparations.

2.2. Immersion processes

Two types of immersion processes were conducted: one was copper immersion coating in a solution that contains hydrofluoric acid; the other was conducted in solutions only containing hydrofluoric acid (HF) at various concentrations. In this study, the former is referred to as the 'copper immersion coating' and the latter the 'HF etching process'.

2.3. Specimen preparation and surface pretreatment

2.3.1. Specimen for immersion processes

For both immersion processes AZ91D samples of 8×10×1.5 mm dimension were used. The samples was pre-treated by a glass beading process in which all surfaces of the sample were blasted with glass beads for 10 seconds at a pressure of 450 kPa. The stream of glass beads bombarded the sample in the normal direction to the surface from a distance of about 10 cm. The sample was then rinsed in isopropanol for 6 minutes with sonication to remove particles adhered to the surface. Finally, alkaline degreasing was performed in a 60g/L NaOH + 10g/L Na_3PO_4 aqueous solution at $75^{\circ}C$ for 6 minutes. After alkaline degreasing the sample was thoroughly rinsed in de-ionized water and immediately transferred into solutions for copper immersion coating or HF etching processes.

2.3.2. Specimen for electrochemical characterization

For electrochemical measurements, including OCP and EIS, AZ91E samples of 10×10×20 mm were used. The sample surfaces were sealed using epoxy resin, except for a 1×1 cm^2 effective working area. The sealed samples were then polished using 320 grit wet emery paper followed by glass beading, isopropanol cleaning, and alkaline degreasing. After thoroughly rinsing in de-ionized water the samples were immediately transferred into solution for the electrochemical measurements.

2.4. Open circuit potential (OCP) and electrochemical impedance spectroscopy (EIS)

OCPs were recorded versus time in a cell with two electrodes, a working electrode and a reference electrode. For EIS a cell fitted with three electrodes, working electrode, counter electrode (Pt gauze with large surface area of ca. 10 cm^2) and reference

electrode, was employed. The reference electrode used was Ag/AgCl/KCl (3M), 0.21V vs. RHE at 25°C, connected to the electrolyte through a salt solution bridge of 3M KCl. All potential values reported in this paper are referenced against the Ag/AgCl/KCl (3M), unless specified otherwise. The distance between the reference electrode and the working electrode was maintained at 0.3 cm during the electrochemical measurements.

The EIS measurements were performed in a frequency range from 100 kHz to 1 Hz, with a bias potential of 0.0 V (vs. OCP) and a 5 mV AC perturbation. An EG&G 273A potentiostat was used, coupled with a M5210 lock-in amplifier. The impedance spectra were fitted using a simple Powersine EIS software (EG&G Instruments, Inc.). It is of note that the fitting process only gives the values of resistance (R_p) and depressed angle associated with the fitted circle. The capacitance values were therefore obtained by $C_p = 1/\omega_{max}.R_p$.

2.5. Scanning electron microscopy (SEM)

A Hitachi S3500N Variable Pressure SEM was employed to examine the surface morphologies of the immersion coating. The images were collected in two modes: secondary electron (SE) and back scattered electron (BSE). Copper coating coverage was measured by processing the images, obtained from BSE mode, with an Image – pro Plus software.

2.6. X-ray photoelectron spectroscopy (XPS)

XPS analyses were carried out using a Kratoes Axis Ultra instrument. Monochromatic Al Kα X-rays were used and the pressure in the spectrometer was ~ 10^{-9} Torr. Binding energy was referenced to the C 1s peak at 285 eV and the spectrometer was calibrated with Cu $2p_{3/2}$ at 932.62 eV and Au $4f_{7/2}$ at 83.96 eV. Spectral deconvolutions were performed after a Shirley background subtraction.

3. Results

3.1 Open circuit potential (OCP)

The change in potential with time during the immersion processes was monitored to study the electrochemical behavior of magnesium alloy during the HF etching process and the copper immersion coating.

3.1.1 HF etching process

Figure 1 illustrates the results obtained during HF etching process in various HF concentrations between 2.2M and 5.5 M. Generally, after immersing the sample into solution, the measured OCP gradually shifts to a more noble value (the plateau potential), attributed to the build up of a surface film on magnesium alloy [20]. Whilst the time for the potential to reach the plateau value is little affected by the HF concentration, the plateau potential is increased with the increase of HF concentration. In the higher hydrofluoric-containing bath (e.g. 5.5M HF) the plateau potential

was – 0.8 V. In 2.2M HF, however, it only attained approximately -1.0 V. Shown in Figure 2 is the effect of temperature on OCP for 3.3 M hydrofluoric acid. It is observed that the plateau potential during the HF etching process increases with increasing bath temperature.

3.1.2 Copper immersion coating

OCP – time curves were also collected during copper immersion coating in various bath conditions, as shown in Figures 3-5. Similar to the HF etching process, the open circuit potential during copper immersion coating shifts to a more noble value with increasing coating time at the initial stage and subsequent plateaus. However, the time for the potential to reach the plateau value during copper immersion coating (e.g. Figure 3) is much shorter than that recorded during HF etching process (Figure 1). More significantly, the plateau potentials recorded in copper immersion coating jumped to approximately 0.1V, close to a potential of

Cu/Cu^{++} redox reaction (~ 0.34V, equation 2), indicating the presence of surface coatings [9, 21].

The effect of HF concentration is significant in terms of both the plateau potential and the time for the potential to reach the plateau value, as observed by comparing the plot for 2.2 HF concentration bath with the curves for the other concentrations (Figure 3). In addition, the plateau potential attained during copper immersion coating is also related to the copper ion concentration in the bath, as shown in Figure 5. It seems that the OCP is not significantly affected by temperature (Figure 4).

Overall, for both the HF etching process and the copper immersion coating, the OCP results show changes in potential vs. time under various conditions. Theses changes reflect information originated from the surface film formation and coating process. However, a realistic interpretation of such information requires input from other experiments (e.g. EIS, XPS, SEM, etc.).

3.2 Electrochemical impedance spectroscopy (EIS)

EIS measurements were conducted to obtain more information on

HF etching process. Shown in Figures 6 are the impedance spectra

in 3.3M HF containing bath at various temperatures between $25^{\circ}C$

and $70^{\circ}C$. The spectra are characterized by a capacitive loop in the

frequency range studied. A simple, one time constant equivalent

circuit (the insert, Figure 6) may be applied to represent the

capacitive loop, i.e. a solution resistance, R_s, in series with a

parallel RC circuit with a resistance, R_p, and a capacitance, C_p. The

values of the R_p and C_p derived, by fitting the semicircles using a

Powersine EIS software, are plotted against HF temperature or

concentration, as shown in Figures 7 and 8.

Capacitances (C_p) obtained in this study, range between 8- 18

μC cm^{-2} (Figures 7 and 8). The values are below that anticipated

for a double-layer capacitance (around 50 μC cm^{-2} [22]).

Generally, such capacitance values were attributed to both a charge

transfer and a film effect [22, 23]. In this study, the impedance

measurements were performed after the magnesium samples were immersed in the solution for 90 seconds. The period for the impedance measurement coincided with the plateau stage on the OCP plots (Figures 1 and 2). During this period, the surface film had already built up. The capacitance obtained was therefore mostly attributed to the film effect and the associated R_p essentially represents the film resistance. As such, the data show that, with increase of both temperature (Figure 7) and HF concentration (Figure 8), the film resistance, R_p, is increased.

The EIS results are in good agreement with the OCP measurements for HF etching process. They confirm the film formation on the magnesium alloy surface, which was characterized using XPS analysis, as will be presented below.

3.3. X-rays photoelectron spectroscopy (XPS)

General survey spectra from XPS measurements of the magnesium surface treated before and after HF etching process are shown in

Figure 9. It detected magnesium, aluminum, fluorine and oxygen as the main composition of the surface film. The presence of sodium, chlorine, sulfur and silicon is attributed to glass beading and the subsequent degreasing process in alkaline solution. From the general survey spectra, it is obvious that before HF etching, the magnesium surface consists of magnesium and aluminum oxide/hydroxide. After HF etching process, a fluorine peak appeared at approximately 686 eV, indicating presence of fluoride.

The surface concentration of different elements in the magnesium surface film measured from XPS is listed in Table 2, from which a number of conclusions can be drawn. First of all, a replacement of surface oxide/hydroxide by fluorides occurs during the HF etching process (compare Sample #00 to #01), consistent with Fairweather [5]; Secondly, the application of alkaline-degreasing process after glass beading seemed not to significantly affect the surface composition formed from the subsequent HF etching process (Sample #01 to #02); Finally, fluorine content in

surface film was increased (while oxygen decreased) with the increase of either HF concentration (Sample #02 to #03) or temperature (Sample #02 to #04).

EDS measurements were also carried out for the quantitative analysis of surface composition at acceleration voltages of 10 KV and 20 KV respectively. The resulted data are listed in Tables 3 (10KV) and 4 (20KV). By comparing the data measured from XPS and EDS, it is expected to obtain more information for the concentration change of the selected elements and their depth profile in the film from the top surface. While XPS, a surface specific tool, has a sampling depth of approximately several nanometers, EDS explores about several micrometers that could be significantly reduced by decreasing the initial electron beam energy (acceleration voltage). Tables 2, 3 and 4 show that, with increasing sampling depth, magnesium content under various treatment conditions is increased while oxygen and fluorine are decreased. It is interesting to note that aluminum content in surface

film first increases then decreases as the sampling depth increases. This suggests the presence of an intermediate layer with an enrichment of aluminum between the top surface and the substrate, which will be discussed latter.

In order to analyze the chemical states in the surface film, peak fittings for the high resolution XPS spectra of Mg 2p, O1s and F 1s core level regions were carried out, as shown in Figure 10. To perform the fitting process, only one peak was needed to fit the spectra for F 1s, but three peaks were required for Mg 2p and two for O 1s [24]. Table 5 summarizes the fitting results, which give not only the absolute binding energy (BE) of different core levels at various conditions, but also the difference of BEs between the levels. By using the difference of BEs, many problems in choosing an appropriate reference level can be avoided when comparing the results from various experiments and the literature.

For Mg 2p core level region the spectra is deconvoluted into three peaks, Mg2p BE(I), Mg2p BE(II) and Mg2p BE(III). The

O1s spectrum is fitted with two peaks, O1s BE(I) and O1s BE(II) (Figure 10). According to Verdier et al [24], the Mg2p BE(I) is related to O 1s BE(I), whilst the higher binding energy Mg2p BE(II) is related to F 1s. The difference, $BE_{O1s\ BE(I)-Mg2p\ BE(I)}$, measured between the O 1s BE(I) and Mg2p BE(I) ranges from 481.3 to 481.4 eV (Table 5), which is in good agreement with the previously reported values [24] for a magnesium hydroxide, $Mg(OH)_2$. This suggests that instead of MgO, $Mg(OH)_2$ was present at the surface of different samples. For the higher binding energy, Mg2p BE(II), it's BE difference from the fluorine core level, $BE_{F1s-Mg2p\ BE2}$ is between 634.3 and 634.4 eV (Table 5). They could be ascribed to $Mg(OH)_{2-x}F_x$ type magnesium hydroxyfluoride, consistent with Verdier [24]. Furthermore, another peak, Mg2p BE(III), was measured, having a binding energy of 53.1 to 53.3 eV. It's BE difference to fluorine core level, $BE_{F1s-Mg\ 2pBE3}$ is 633 to 633.2 eV, suggesting the presence of MgF_2 at the surface film according to the BE difference reported for a standard MgF_2 [24].

The oxygen spectra (Figure 10) also shows a high binding energy peak, O1s BE(II), at approximately 534 eV for the different samples, which could be ascribed to oxygen atoms bound to carbon atoms in the contamination layer [25, 26].

3.3 Surface morphology and copper coverage

3.3.1. HF etching process

Scanning electron microscopy was employed to examine the surface morphology of magnesium alloy treated under various conditions. Shown in Figure 11 and 12 are the secondary electron images obtained after the HF etching process. For comparison, the image obtained from a sample before HF etching process is also presented (Figure 11f). It shows that the surface morphologies formed by HF etching process exhibit a typical "mud-like" texture. "Mud-like" texture is usually produced by precipitation of corrosion products. As corrosion products dehydrate, the precipitate contracts, forming cracks.

In this study the observed Mud-like texture was formed by the precipitation of magnesium-fluoride species generated during the HF etching process. This may give an indication of the significance of magnesium dissolution. Thus, the effect of temperature on the surface texture of magnesium after the HF etching process is significant: more dissolution of magnesium is observed at lower temperature (e.g. 25°C) than higher temperature (e.g. 70°C). In particular, there is little difference between the Images of Figures 11e, HF treated at 70°C, and 11f, before HF treatment, which is evident that magnesium dissolution at 70°C rarely occurs. With regard to the HF concentration effect (Figure 12), it is also clear that the dissolution of magnesium in the higher HF concentration (e.g. 5.5M HF) is less observable than that in lower HF concentration (e.g. 1.1 M HF).

3.3.2. Copper immersion coating

The back scattered electron images of copper immersion coating are presented in Figures 13 and 14, showing the effects of HF concentration and temperature, respectively. The coating coverage derived from these images is shown as the inserts in the corresponding figures. Figure 13 indicates that surface coverage first increases with increasing HF concentration and then decreases after reaching a maximum point at 3.3M HF. With regard to temperature effect it is clear that the copper surface coverage decreases with increasing bath temperature (Figure 14).

4. Discussion

4.1 Surface film formation during HF etching process

From the experimental results, it is clear that both temperature and HF concentration significantly affect the film formation on the magnesium surface during the HF etching process.

According to the OCP results (Figures 1 and 2), the value of plateau potential ranges from -1.0 to -0.8 V, depending on HF

concentration and bath temperature. The standard potential of electrode reaction for Mg/Mg^{2+} is -2.375 V vs. SHE [15]. In chloride aqueous solutions the actual corrosion potential of magnesium is usually increased to $-1.5 \sim -1.7$ V vs. SHE, attributable to the formation of a surface film of $Mg(OH)_2$ or MgO [27,4]. In this study, the further increase in OCP in the presence of fluoride instead of chloride is due to the fluoride containing species in the film.

A comparison of XPS and EDS results suggests the presence of an intermediate layer with enrichment of aluminum between the outer surface and the substrate. The surface film formed prior to HF etching (Sample #00) can therefore be proposed to have a structure of $Mg(OH)_2$/Mg-Al-oxide/substrate, consistent with the air-formed film structure on magnesium alloy surface [3, 28]. After the HF etching process the resulting film structure is expected to consist of an outer layer rich in fluorine (MgF_2-$Mg(OH)_{2-x}F_x$), an intermediate layer ($Mg-Al(OH)_{2-x}F_x$) and an inner layer of Mg-Al

oxide rich in aluminum. It ought to be mentioned that there might not be distinct boundaries between the layers as the composition might vary gradually from one layer to another.

To understand the outer layer and the inner layer the stability of magnesium and aluminum in hydrofluoric acids should be taken into consideration. In HF solution (pH ~ 2-3), aluminum is known to be unstable and may form AlF_6^{3-} complexes, dissolving into solution [29-31]. In contrast, magnesium may form intermediate species, MgF^+, subsequently converted to MgF_2 and precipitated as a surface film [20, 27]. The resulted MgF_2 may also be followed by a F^-/OH^- exchange or hydration process, resulting in a more stable surface film containing $Mg(OH)_nF_{2-n}$ [27]. This explains why the aluminum content is low in the outer layer, consistently shown for all samples after the HF etching process (Table 2). For the inner layer where the HF solution cannot contact directly, Al_2O_3 is expected to accumulate preferentially at the alloy/film interface because of the stronger affinity of aluminum for oxygen

than magnesium [28]. It might be reasonable to assume that the inner layer is much more compact than both the intermediate layer and the outer layer as a result of selective dissolution of aluminum. As such the protective nature of the surface film formed during HF etching process may be mostly attributable to the inner layer and the intermediate layer, as the outer layer remains loose after selective dissolution.

SEM shows that the surface film is more compact at higher temperature (Figure 11) or in the solutions with higher HF concentration (Figure 12). Such trends are also reflected by the OCP results in terms of both the plateau potential and the time for positive potential shift prior to reaching the plateau values (Figures 1 and 2). This is also consistent with the EIS results through the observed reduction of R_p due to a film formation process as HF concentration or temperature increases (Figures 7 and 8). The film formation on the magnesium alloy is closely correlated with copper immersion coating, which will be discussed below.

4.2 Copper immersion coating – HF concentration dependence

Theoretical conditions for copper immersion coating in aqueous solution may be determined from the Pourbaix diagrams of copper-water system and magnesium-water system [32]. For the deposition of copper to occur, the potential of the substrate must be in the region where metallic copper is stable and the magnesium must be in the dissolving region. However, it was observed that during a simple experiment performed in an aqueous copper-containing bath, copper reduction was accompanied by violent gas evolution and magnesium dissolution. The immersion coating process was not able to automatically stop and the resulted copper deposition was un-uniform, non-adherent and spongy with low coverage.

According to the discussion in Section 4.1, hydrofluoric acid is beneficial to the surface film formation on magnesium, which protects magnesium from violent dissolution. It is therefore added

to the immersion-coating bath to render a control of the magnesium dissolution, hence, copper deposition. The surface morphologies obtained from the copper immersion coating in the hydrofluoric acid containing baths are depicted in Figure 13 and 14. The morphologies showed coated areas (white) and uncoated areas (dark). During copper immersion coating, the magnesium surface consists of a mosaic of anodic and cathodic sites. The magnesium dissolves on the anodic sites, resulting in copper deposition occurring on the cathodic sites.   The deposition process continues until the entire substrate is covered with copper and fluoride/hydroxide film. At this point, anodic dissolution virtually ceases resulting in the termination of immersion deposition. This can be manifested by the coverage-time plot [14]. According to the above discussion a model, shown in Figure 15, depicts the immersion coating process.
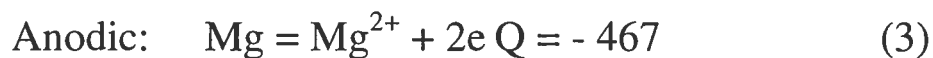
The relation between HF concentration and copper surface coverage is given in Figure 13, which shows a peak at

approximately 3.3M HF. This can be explained according to the proposed model: in a lower HF containing bath (e.g 1.1M HF), the surface film formed on magnesium possessed a loose and discontinuous feature (Figure 12 a) with poor protective characteristic. The dissolution of magnesium is therefore violent, resulting in non-adherent and spongy copper deposits that were subsequently partially removed from the substrate surface by violent hydrogen evolution. With an increase of HF concentration, the surface film formed became increasingly more dense and compact (Figure 12) with a higher content of fluoride species (Table 2-4). Such a compact film, simultaneously formed during copper deposition, not only prevented violent magnesium dissolution but also enabled copper to deposit as fine and adhesive crystallites (Figures 13 b-c). With the further increase in HF concentration beyond the maximum point of surface coverage, however, copper deposition was only able to take place at a very early stage because the rapid film formation limited the available

anodic sites on the surface. As a result, a decrease in copper

coverage is observed (Figure 13).

4.3 Copper immersion coating – temperature effect

Figure 14 indicates that the surface copper coverage on the

substrate decreased with the elevation of bath temperature. For an

understanding of the mechanism of such temperature effects, the

enthalpy change of the reactions involved during copper

immersion coating is discussed below:

$$\text{Anodic:} \quad Mg = Mg^{2+} + 2e \quad Q = -467 \tag{3}$$

$$\text{Cathodic} \quad Cu^{2+} + 2e = Cu \quad Q = -64.9 \tag{4}$$

$$2H^+ + 2e = H_2 \quad\quad Q = 0.0 \tag{5}$$
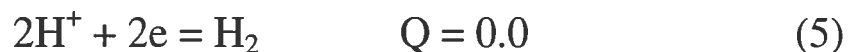
Where, Q is the standard formation of enthalpy (kJ mol^{-1}) for

the reactions at 298 .15 K. The formation of the corrosion product,

Mg^{++}, subsequently reacts with F$^-$ or water to form a surface film

[12,27]:

$$Mg^{++} + F^- = MgF_2 \qquad Q = 13$$

(6)

$$Mg^{++} + H_2O = MgO + 2H^+ \quad Q = 151 \qquad (7)$$
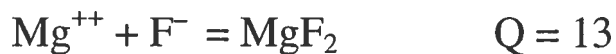
As indicated, the reactions (3) and (4) are exothermic, while (6)

and (7) are endothermic. Therefore, increasing temperature is

unfavourable to both magnesium dissolution and copper reduction,

whilst the film formation on the uncoated areas is favoured by

either forming fluoride or oxide film.

5. Conclusions

1. Formation of a surface film on magnesium alloy in

hydrofluoric acid is proposed to have a structure composed of an

outer layer rich in fluorine, an intermediate layer and the inner

layer rich in aluminum, presented as $(MgF_2\text{-}Mg(OH)_{2\text{-}x}F_x)$ / (Mg-

$Al(OH)_{2\text{-}x}F_x$) / Mg-Al oxide / substrate.

2. The surface film formation on AZ91 magnesium alloy was

found to affect the Cu immersion coating process. The

effectiveness of surface film depends on the kinetics of the chemical/electrochemical reactions occurring during the immersion coating process.

3. Both HF concentration and bath temperature have a significant effect on the copper immersion deposition. Whilst the HF concentration effect is attributed to the surface film formation on uncoated areas, the temperature dependence is mostly attributed to the enthalpy change of the reactions involving in the coating process.

4. A model for understanding the copper immersion coating process is depicted. This model is based on results from the XPS and EDS analyses, morphology observations and electrochemical evidence.

Acknowledgement

References

1. Kainer, Magnesium alloy and technologies, ed.: K. U. Kainer, Trans. Frank Kaiser, Wiley-VCH GmbH & Co. KGaA (2003)

2. R. Ambat, N.N. Aung and W. Zhou, J. Appl. Electrochem. **30** (2000) 865.

3. G.L. Makar and K. Kruger, J. Eelctrochem. Soc. **137** (1990) 414.

4. G. Song and A. Atrens, Advanced Engineering Materials **1** (1999) 11.

5. E.F. Emley, Principle of Magnesium Technology, CH. XX, Pergmon Press New York(1966).

6. G. Song, A. Atrens, D. John, X. Wu and J. Nairn, Corrosion Science **39** (1997) 1981.

7. J. E.Gray and B. Luan, J. of Alloys and Compounds **336** (2002) 88.

8. J.H. Chen, C.C. Chang and T.S. Lee, "Pretreatment for Plating on Magnesium Alloys," AESF SUR/FIN' 91, (1991) 754.

9. J.K. Dennis, M.K.Y.Y. Wan and S. Wakes, Trans. IMF. **63** (1985) 74.

10. W.A. Fairweather, Trans. IMF. **75** (1997) 113.

11. A.K. Sharma, M.R. Suresh, H. Bhojraj, H. Narayanamurthy and R.P. Sahu, Metal Finishing (USA) **96** (1998) 10.

12. Y. Xiang, W. Hu, X. Liu, C. Zhao and W. Ding, Trans. IMF. **79** (2001) 27.

13. Sakata, Y., "Electroless Nickel Plating Directly on Magnesium Alloy Die Castings," 74th AESF Technical Conference, pp15 (1987).

14. L. X. Yang. B. Luan, W.J. Cheong and D. Shoesmith, J Coating Technology Research, accepted, (2004).

15. Stojek Z., the Electrical Ddouble Layer and Its Structure, in Eelctroanalytical Methods, Guide to Experiments and Applications, ed. F. Scholtz, Springer (2002).

16. R. P. Kallenbanch, US patent 3,672,976 (1972).

17. M. Kanungo, V. Chakravarty, K. G. Mishra and S.C. Das, Hydrometallurgy **61** (2001) 1.

18. B. Luan, T. Le and J. Nagata, Surface & Coating Technology **186** (2004) 431.

19. S. G. Robertson and I. M. Ritchie, J Appl. Eelctrochem. **27** (1997) 799.

20. J.K. Dennis, M.K.Y.Y. Wan and S. Wakes, Trans. IMF. **63** (1985) 81.

21. L. Kouisni, M. Azzi, M. Zertoubi, F. Dalard and S. Maximovitch, Surface & Coating Technology **185** (2004) 58.

22. G. Baril, C. Blanc and N. Pebere, J. Electrochem. Soc. **148** (2001) B489.

23. G. Baril and N. Pebere, Corrosion Science **43** (2001) 471.

24. S. Verdier, N. Laak, S. Delalande, J. Metson and F. Dalard, Applied Surface Science **235** (2004) 513.

25. C. Chen, S.J. Splinter, T. Do and N. S. McIntyre, Surface Science **382** (1997) L652

26. Fuggle, J.C., Surface Science **69** (1977) 581.

27. K.G. Cowan and J.A. Harrison, Electrochimica Acta **25** 899 (1980).

28. G. Song, A. Atrens, X. Wu and B. Zhang, Corrosion Science **40** (1998) 1769.

29. T. Schram, G. Goeminne, H. Terryn, W. Vanhoolst and P. Espen, Trans. IMF

    73 (1995) 91.

30. L. Fedrizzi, F. Deflorian and P.L. Bonora, Electrochimica Acta **42** (1997) 969.

31. T. Xue, W.C. Cooper, R. Pascual and S. Saimoto, J. Applied Electrochemistry **21**

    (1991) 238

32. M. Pourbaix, Atlas of Electrochemical Equilibria in Aqueous Solutions, Pergamon

    Press, London (1966).

List of figures and tables

OCP

Figure 1. OCP / time curves recorded for AZ91 magnesium alloy in HF solutions at 25°C, showing the effect of HF concentration on OCP during the HF etching process.

Figure 2. OCP / time curves recorded for AZ91 magnesium alloy in 3.3M HF containing solutions, showing the effect of temperature on OCP during HF etching process.

Figure 3. OCP / time curves recorded for AZ91 magnesium alloy in HF + 0.67M $CuSO_4$ solutions at 25°C, showing the effect of HF concentration on OCP during copper coating process.

Figure 4. OCP / time curves recorded for AZ91 magnesium alloy in 3.3 M HF + 0.67M $CuSO_4$ containing solutions, showing the effect of temperature on OCP during the copper coating process.

Figure 5. OCP / time curves recorded for AZ91 magnesium alloy in 4.4 M HF + $CuSO_4$ solutions at 25°C, showing the effect of concentration of copper ions on OCP during the copper coating process.

EIS

Figure 6. Typical Nyquist plots recorded for AZ91 magnesium alloy in 3.3M HF bath at various temperatures with a proposed equivalent circuit (the insert). During the experiments the EIS measurement was not started until 90 seconds after the sample was immersed in the solution.

Figure 7. Effect of temperature on film resistance, R_p, and capacitance, C_p, obtained from HF etching process in 3.3M HF. During the experiments the EIS measurement was not started until 90 seconds after the sample was immersed in the solution.

Figure 8. Effect of HF concentration on the film resistance, R_p, and capacitance, C_p, obtained from HF etching process at room temperature. During the experiments the EIS measurement was not started until 90 seconds after the sample was immersed in the solution.

XPS

Figure 9. Survey scans of XPS on AZ91 magnesium alloy surface before (Sample #00) and after (Samples #01) HF etching (see Table 2 for the samples' treatment conditions).

Figure 10. High resolution scans of Mg 2p, O 1s and F 1s on AZ91 magnesium alloy surface under various treatment conditions (Samples #02, #03 and #04, see Table 2 for the samples' treatment conditions).

SEM

Figure 11. Secondary electron (SE) images for AZ91 magnesium alloy after the HF etching process for 10 minutes in 3.3MM HF solutions at various temperatures. (a) 25°C, (b) 35°C, (c) 50°C, (d) 60°C, (e) 70°C and (f) before HF etching.

Figure 12. Secondary electron (SE) images for AZ91 magnesium alloy after the HF etching process for 10 minutes in HF solutions at room temperature. (a) 1.1M HF, (b) 3.3M HF, (c) 4.4M HF and (d) 5.5M HF.

Figure 13. Back-scattered electron (BSE) images for AZ91 magnesium alloy after the copper immersion coating for 10 minutes in HF + 0.67M $CuSO_4$ solutions at room temperature: (a) 2.2M HF, (b) 3.3M HF, (c) 4.4M HF and (d) 5.5M HF. The insert is the plot of copper coverage – HF concentration derived from the BSE images.

Figure 14. Back-scattered electron (BSE) images for AZ91 magnesium alloy after the copper immersion coating for 10 minutes in 3.3M HF + 0.67M $CuSO_4$ containing solutions at various temperature between 25°C and 70°C. The insert is copper coverage – Temperature plots derived from BSE images.

Model
Figure 15. The model for understanding the copper immersion coating process.

Table 1. The nominal chemical compositions of the AZ91D and AZ91E magnesium alloy used in the experiments.

Table 2. XPS concentration of Mg, Al, F and O in the surface film of magnesium alloy with various pretreatment conditions.

Table 3. EDS concentration of Mg, Al, F and O in the surface film of magnesium alloy with different pretreatments (see Table 2 for the samples' treatment conditions). EDS measurements were performed at an acceleration voltage of **10** KV.

Table 4. EDS concentration of Mg, Al, F and O in the surface film of magnesium alloy with different pretreatments (see Table 2 for the samples' treatment conditions). EDS measurements were performed at an acceleration voltage of **20** KV.

Table 5. Chemical shifts (in eV) for Mg 2p, O1s and F1s core level regions for Samples #02, #03 and #04 (see Table 2 for the samples' treatment conditions).
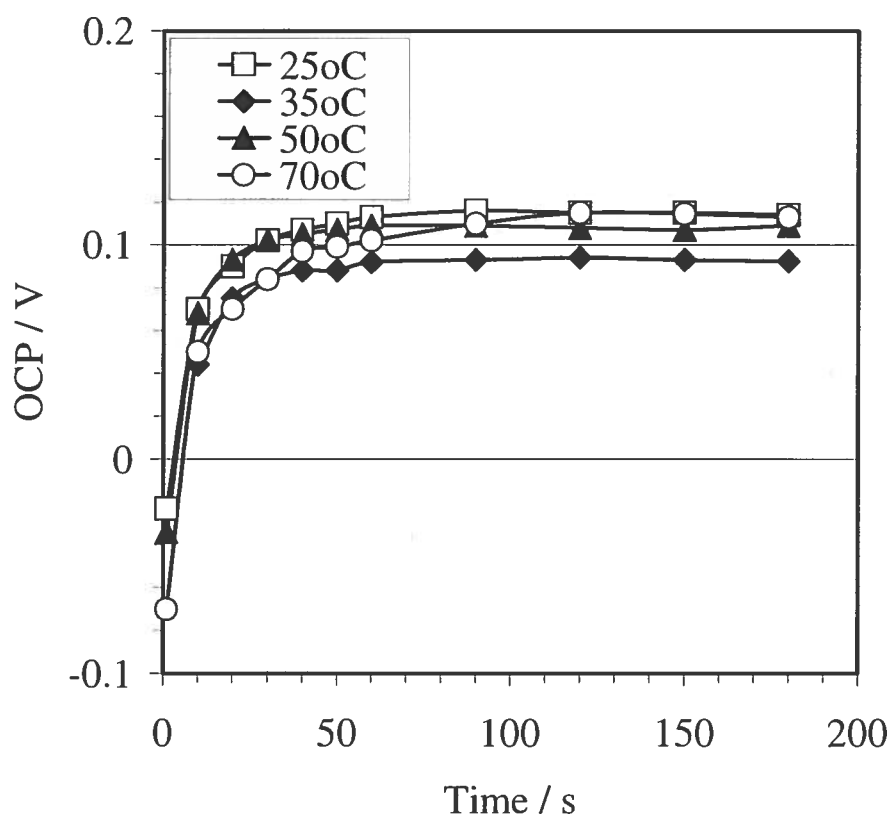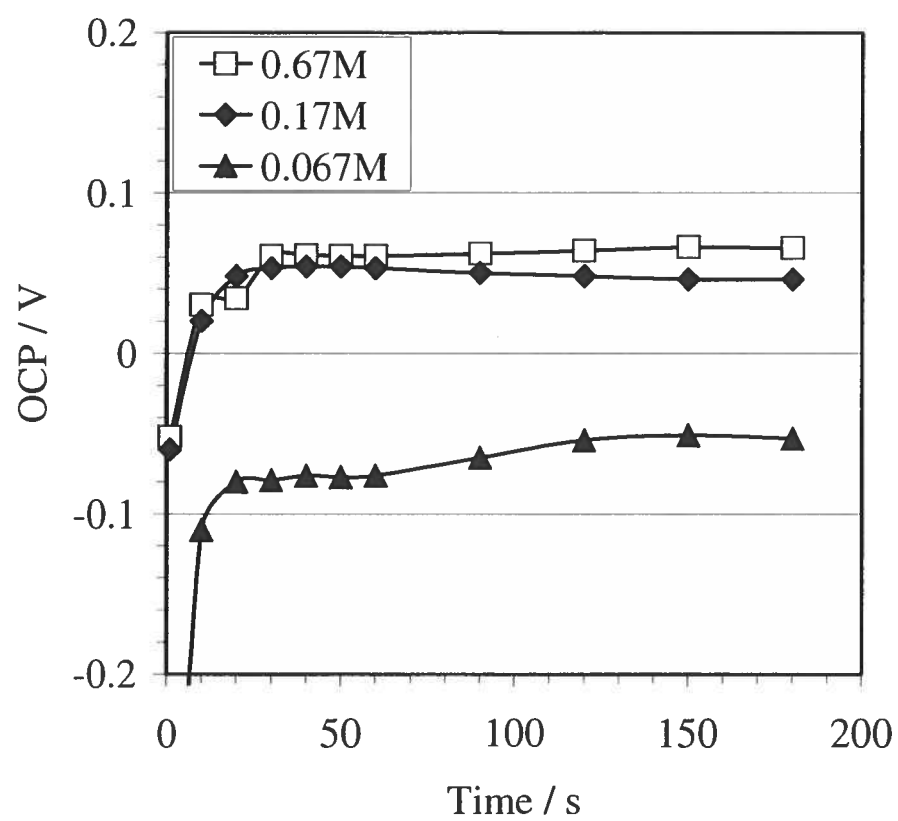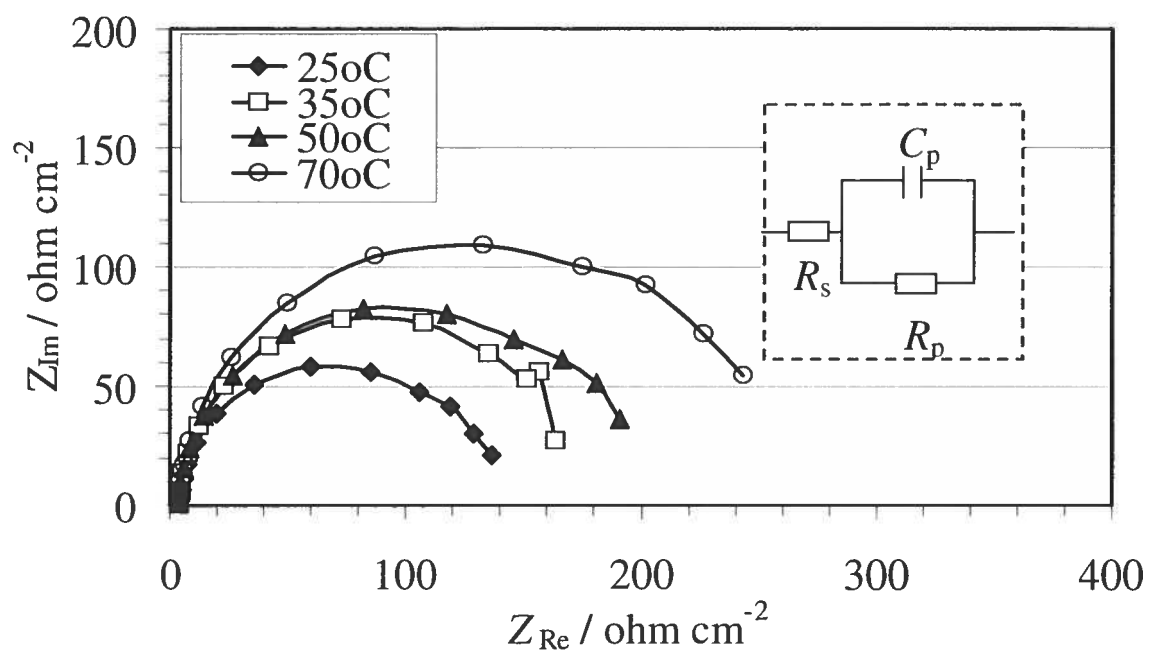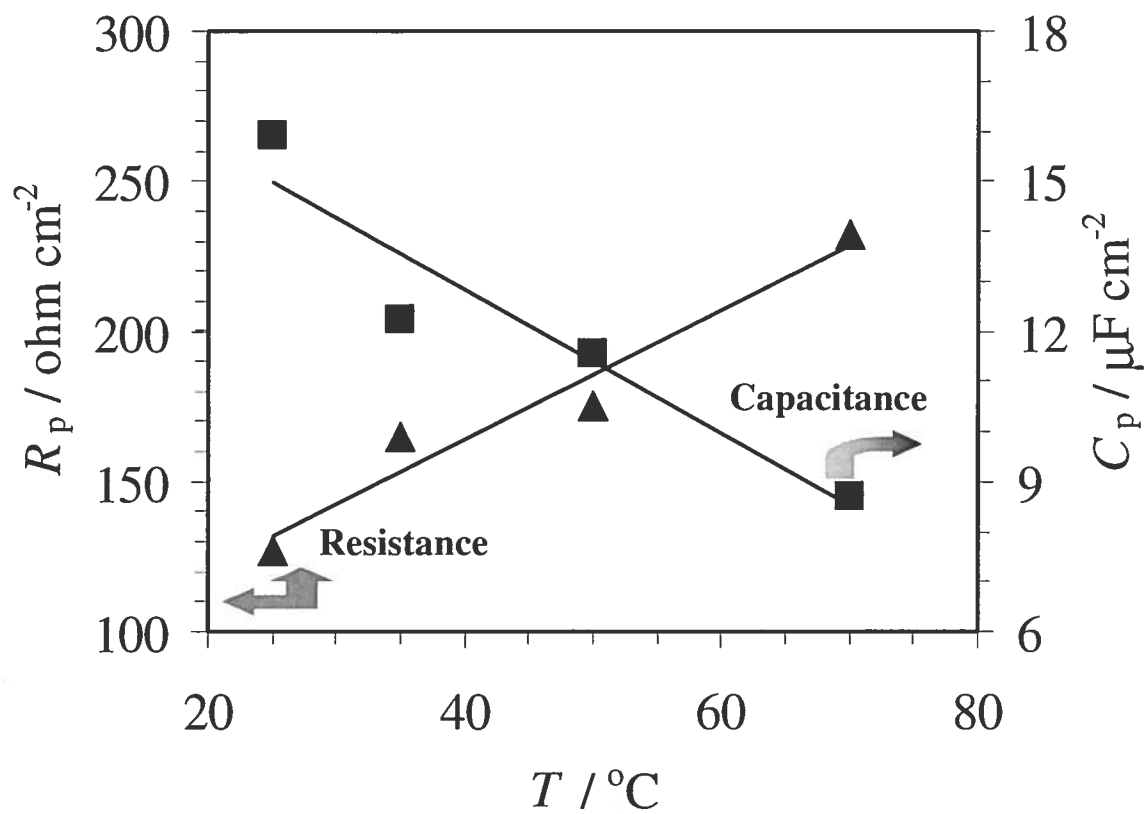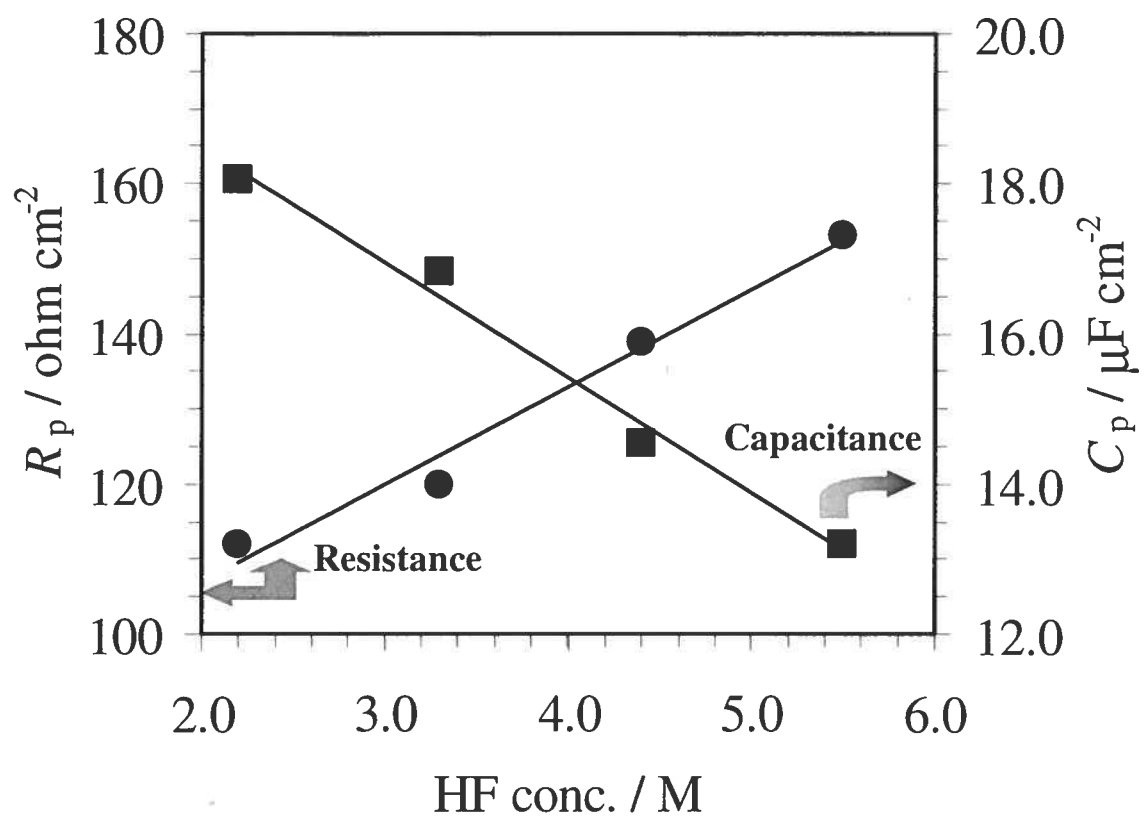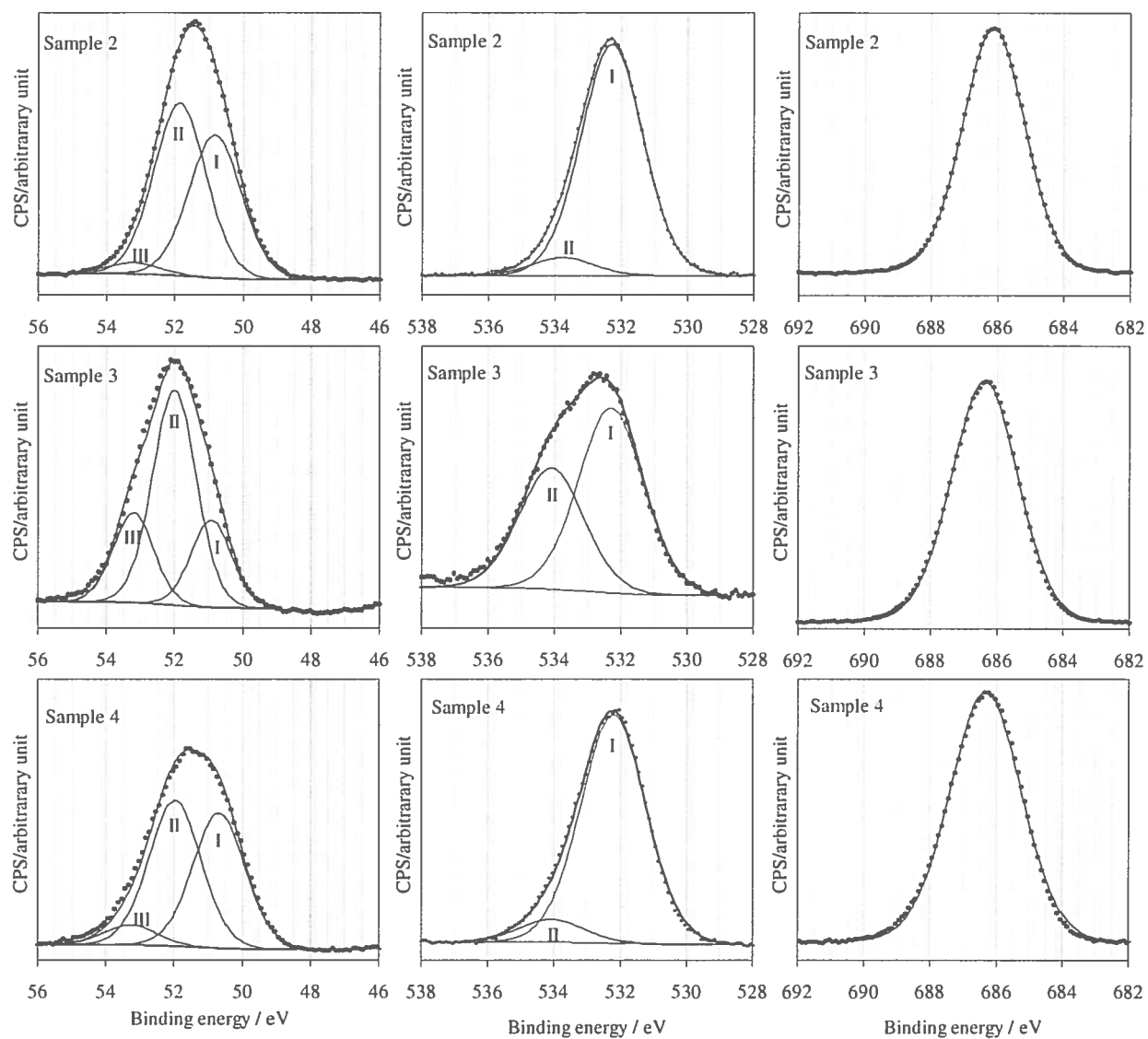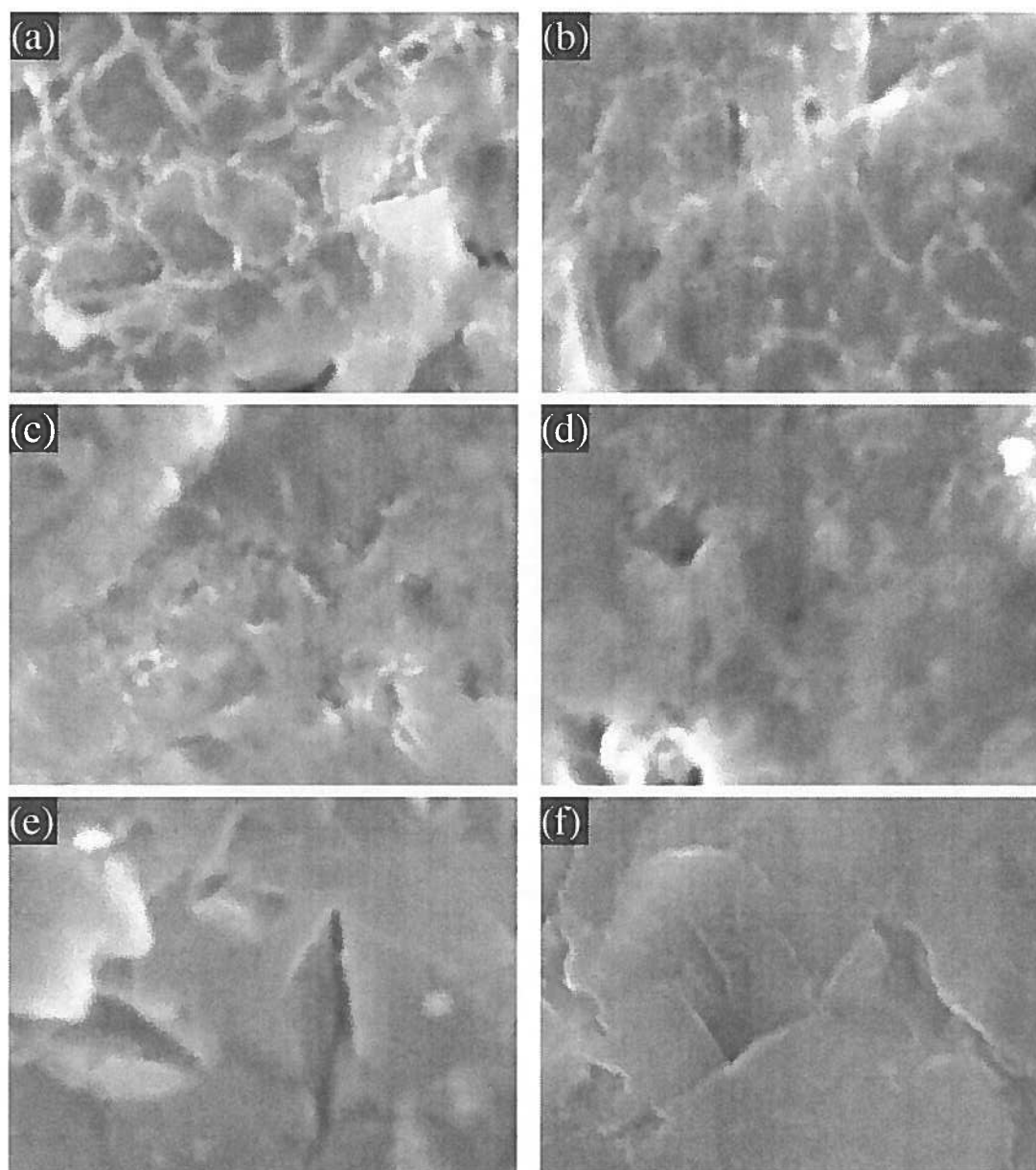
Figures
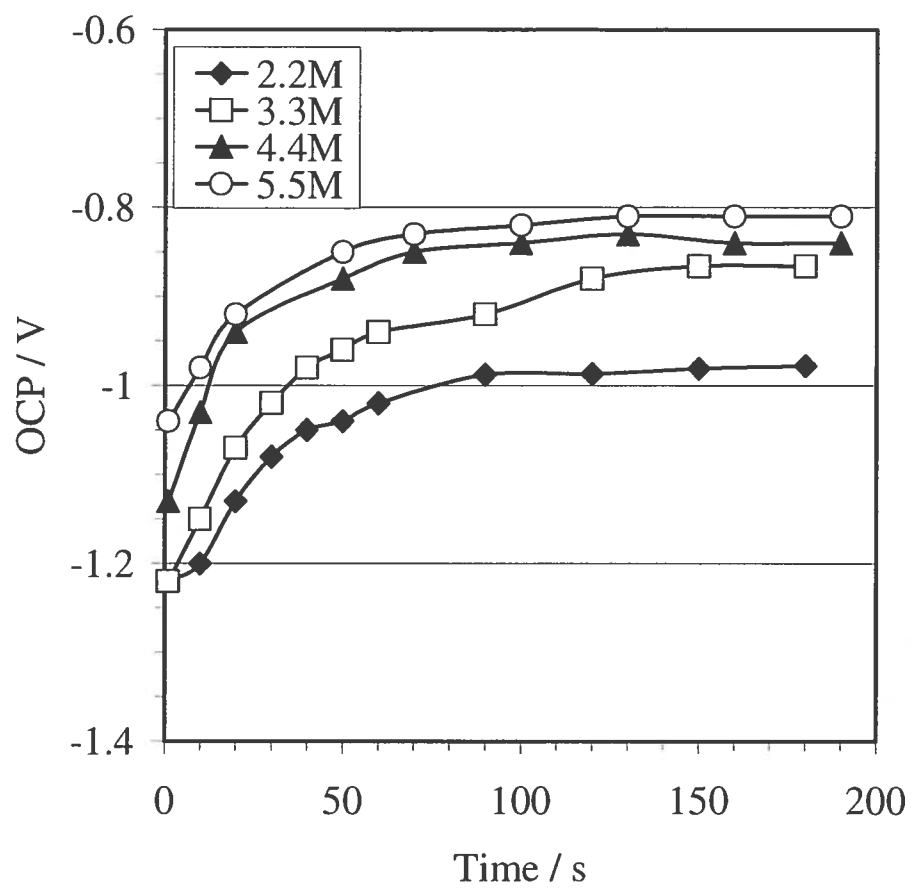
Figure 1
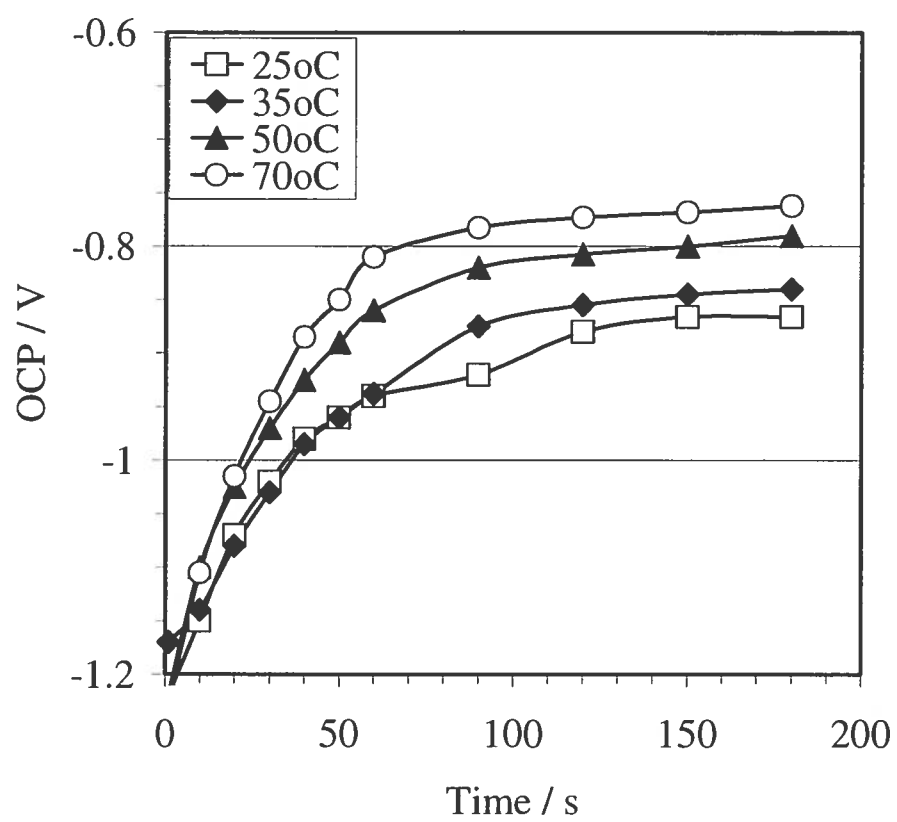
Figure 2
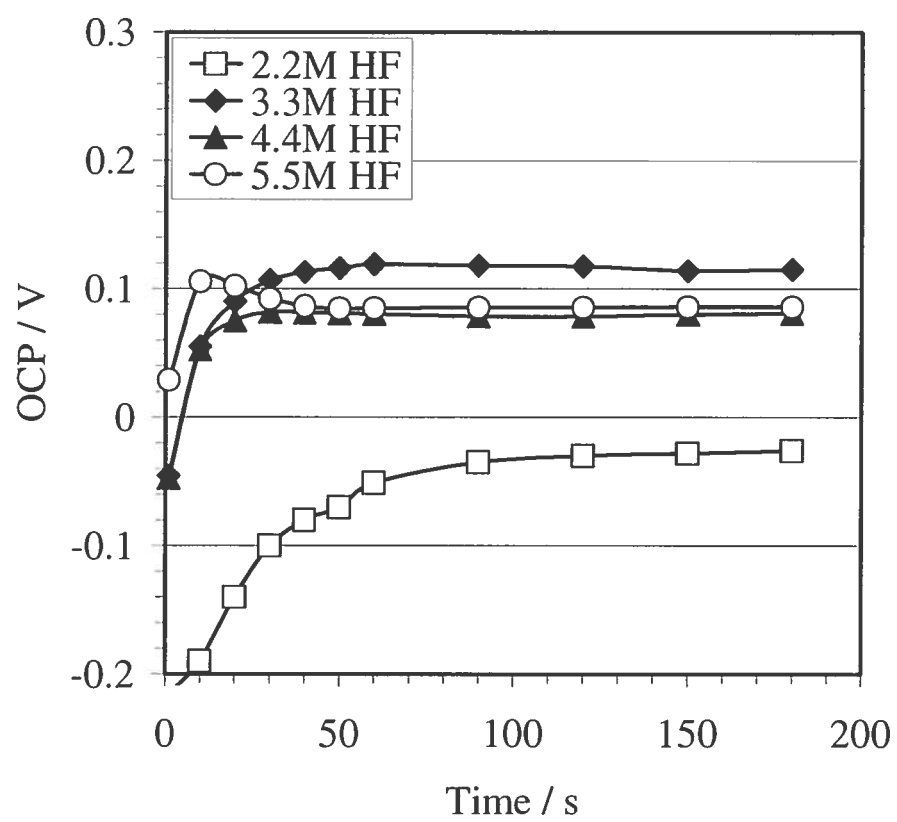
Figure 3

Figure 4

Figure 5

Figure 6

Figure 7

Figure 8

Figure 9

Mg 2p   **O 1s**   **F 1s**

Figure 10

10 μm

Figure 11

10 μm

Figure 12

200μm

Figure 13

200μm

Figure 14

1. Before Cu coating   2. During Cu coating   3. After Cu coating
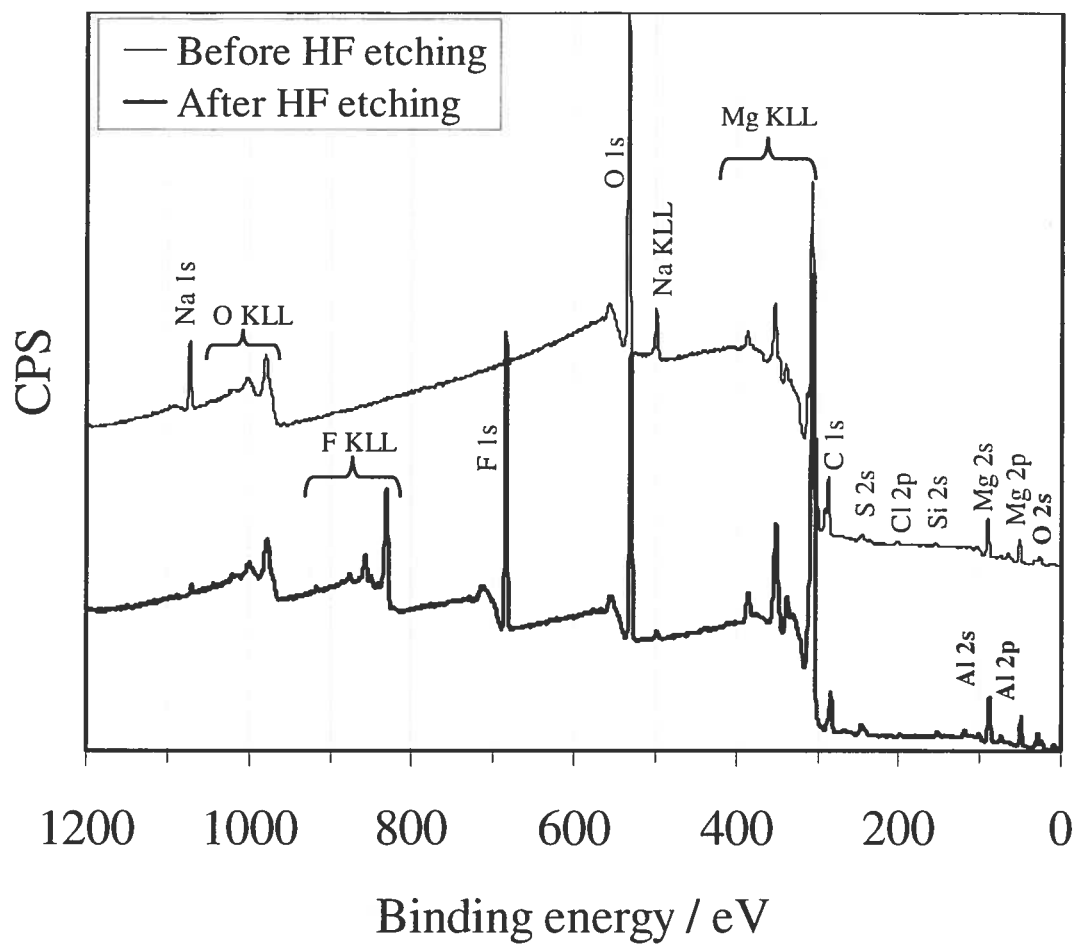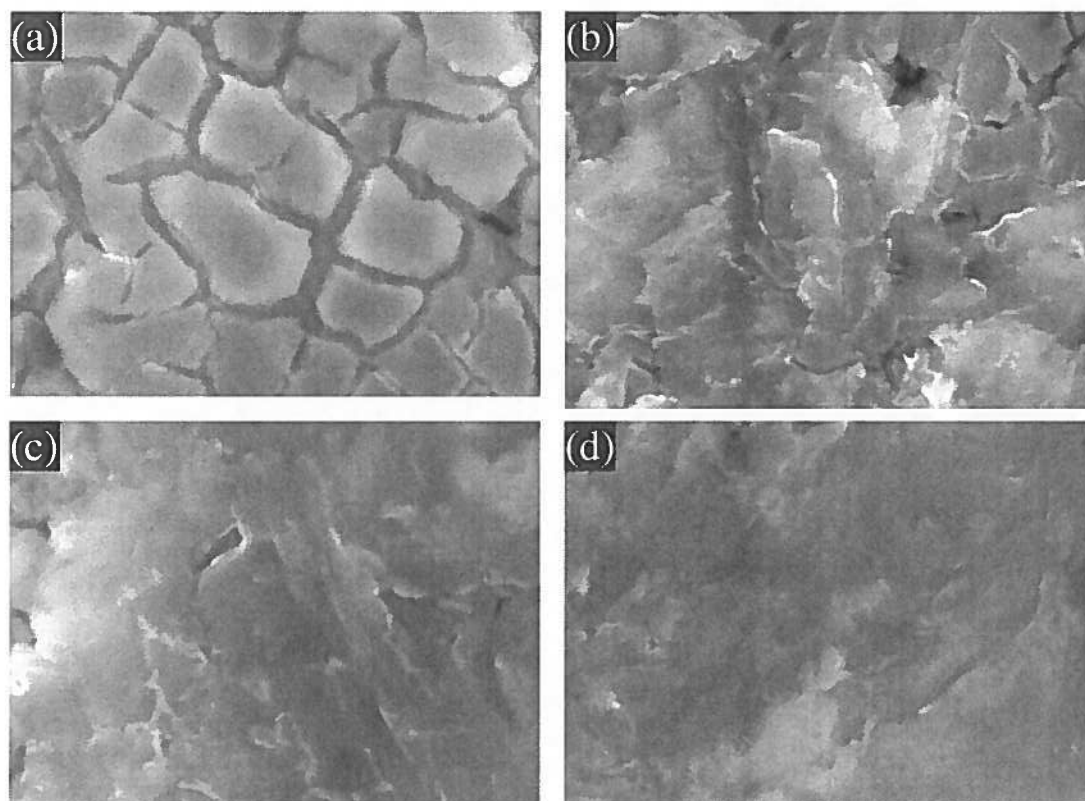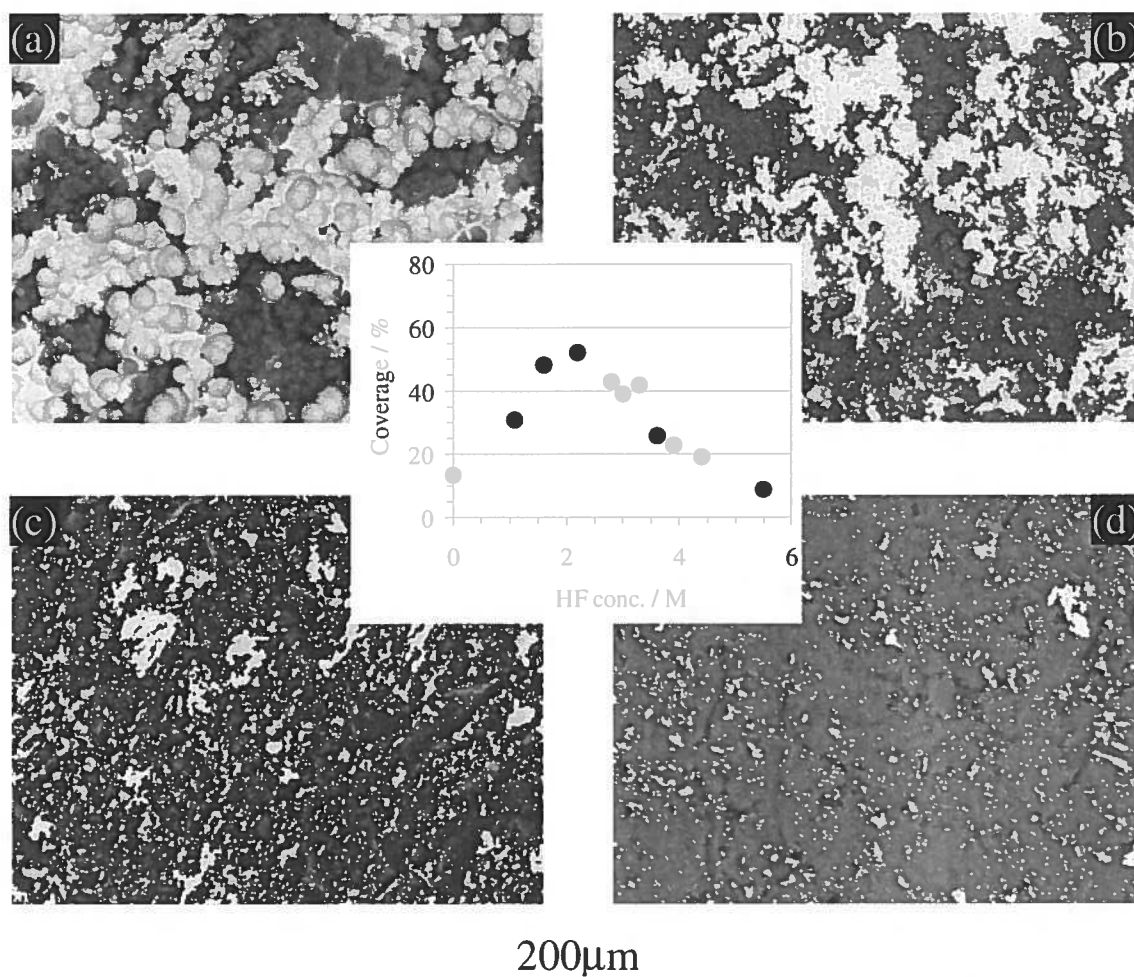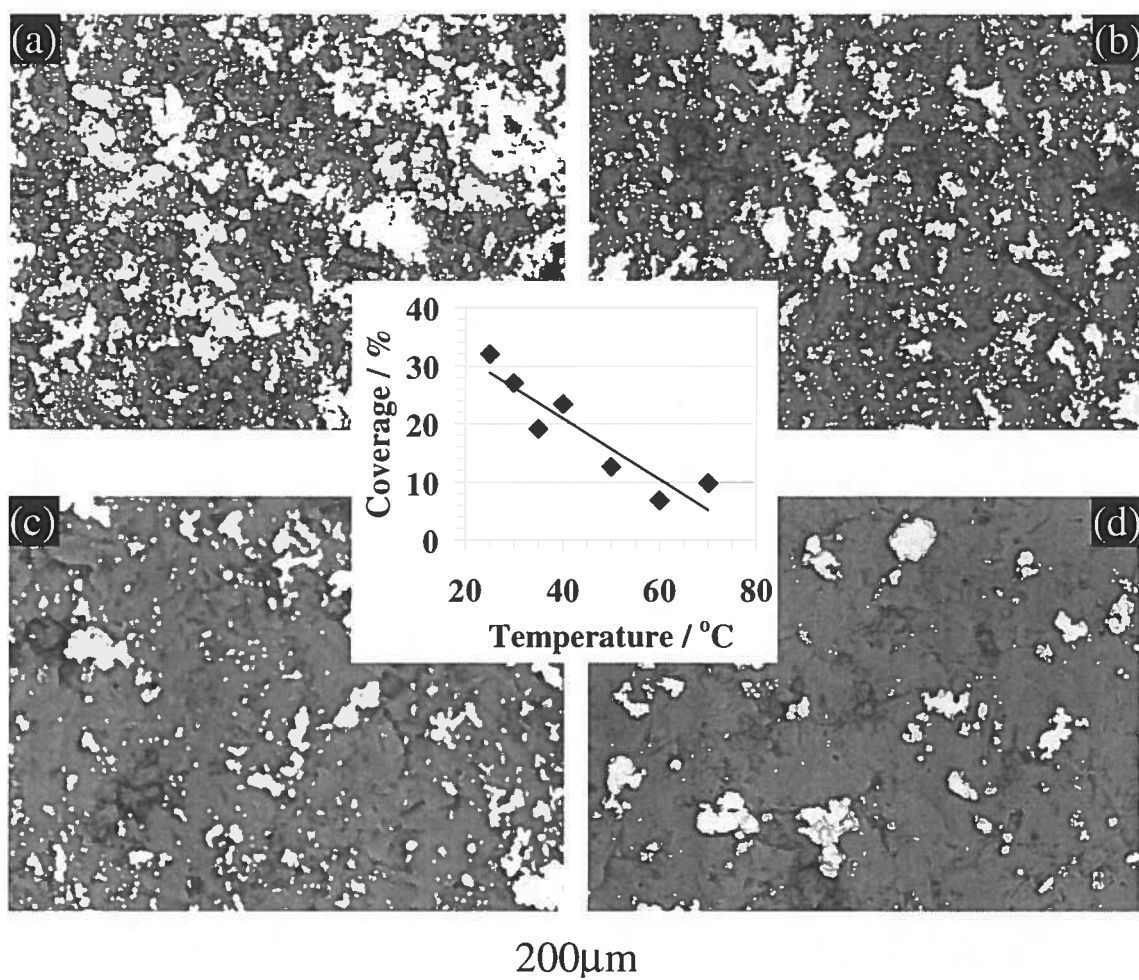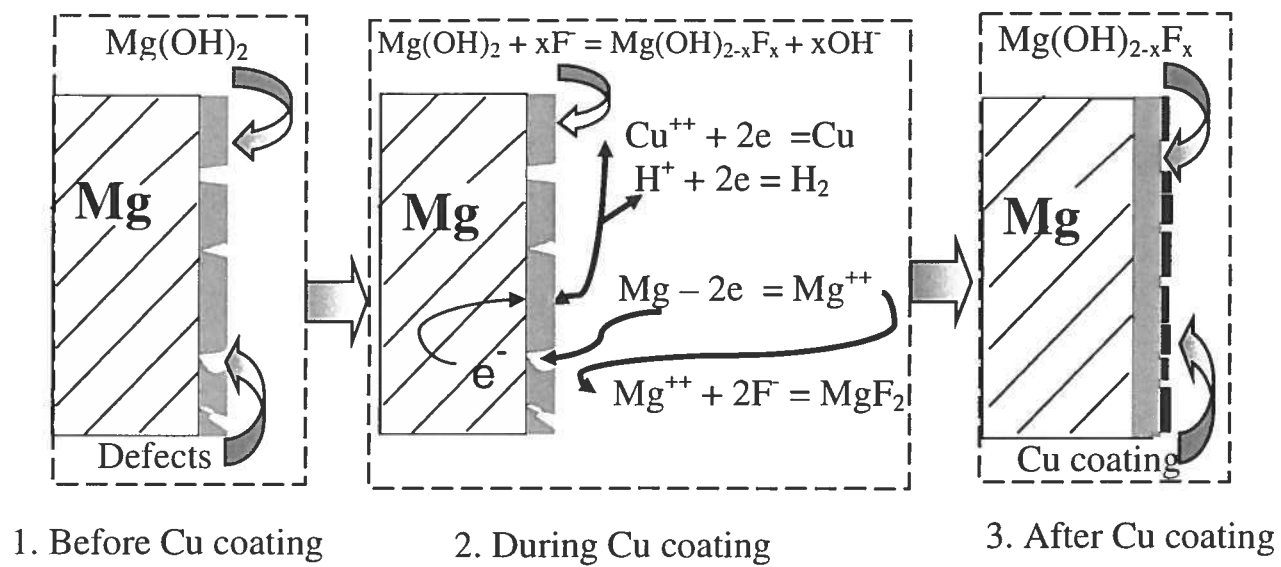
Figure 15

Table 1

	%Al	%Zn	%Mn	%Ni	%Cu	%Si	%Fe	%Be	Other Total
AZ91D[1]	8.5-9.5	0.45 - 0.90	0.17 - 0.40	0.001	0.015	0.05	0.004	0.0005-0.003	NS
AZ91E[2]	8.3-9.2	0.45 - 0.90	0.15-0.50	0.001	0.015	0.2	0.005		0.03

[1] AZ91D was supplied by Norsk Hydro Canada.

[2] AZ91E was supplied by Haley Industries Limited, Canada

Table 2

Sample	Atomic percentage %			
	Mg	Al	F	O
#00	27	0.6	0	72
#01	23	2.0	34	41
#02	24	1.8	37	37
#03	20	1.7	61	17
#04	22	1.8	43	33

#00: AZ91D – glass beading – isopropanol cleaning

#01: AZ91D – glass beading – isopropanol cleaning – 3.3 M HF etching for 10 seconds
     at room temperature

#02: AZ91D – glass beading – isopropanol cleaning – alkaline degreasing
     – 3.3 M HF etching for 10 seconds at room temperature

#03: AZ91D – glass beading – isopropanol cleaning – alkaline degreasing
     – 5.5 M HF etching for 10 seconds at room temperature

#04: AZ91D – glass beading – isopropanol cleaning – alkaline degreasing
     – 3.3 M HF etching for 10 seconds at 70°C

Table 3

Sample	Atomic percentage %			
	Mg	Al	F	O
#00	77	9.1	0.0	14
#01	72	9.3	5.0	13
#02	74	7.6	6.7	11
#03	68	8.8	15	8
#04	70	6.9	10	13

Table 4

Sample	Atomic percentage %			
	Mg	Al	F	O
#00	80	7.7	0.0	13
#01	78	8.2	3.5	10
#02	81	7.0	3.8	9
#03	75	8.4	9.3	7
#04	76	6.8	6.7	10

Table 5

Sample	M 2p BE(I)	M 2p BE(II)	M 2p BE(III)	O 1s BE(I)	O 1s BE(II)	F 1s	O 1s BE(I) – Mg 2p BE(I)	F 1s – Mg 2p BE(II)	F 1s – Mg 2p BE(III)
#02	50.8	51.9	53.1	532.2	533.8	686.3	481.4	634.4	633.2
#03	50.9	52	53.3	532.3	534.1	686.3	481.4	634.3	633
#04	50.8	52	53.2	532.1	534	686.3	481.3	634.3	633.1
Data from	ref.[24]						481.3 to 481.7	634.5 to 634.7	632.9
Ascribed	to						$Mg(OH)_2$	$Mg(OH)_{2-x}F_x$	MgF_2